

A General Method for Conserving Energy and Potential Enstrophy in Shallow-Water Models

RICK SALMON

Scripps Institution of Oceanography, University of California, San Diego, La Jolla, California

(Manuscript received 7 September 2005, in final form 15 March 2006)

ABSTRACT

The shallow-water equations may be posed in the form $dF/dt = \{F, H, Z\}$, where H is the energy, Z is the potential enstrophy, and the Nambu bracket $\{F, H, Z\}$ is completely antisymmetric in its three arguments. This makes it very easy to construct numerical models that conserve analogs of the energy and potential enstrophy; one need only discretize the Nambu bracket in such a way that the antisymmetry property is maintained. Using this strategy, this paper derives explicit finite-difference approximations to the shallow-water equations that conserve mass, circulation, energy, and potential enstrophy on a regular square grid and on an unstructured triangular mesh. The latter includes the regular hexagonal grid as a special case.

1. Introduction

Salmon (2005, hereafter S05) offered a general method for constructing numerical fluid models that, in the inviscid limit, conserve energy and an arbitrary additional invariant related to the potential vorticity. In geophysical fluid dynamics, the conservation of potential enstrophy is thought to be especially important.

The method proposed by S05 relies on the fact that the equations of fluid mechanics fit the Hamiltonian form

$$\frac{dF}{dt} = \{F, H\}, \tag{1.1}$$

where F is an arbitrary functional of the fields representing the state of the fluid, H is the Hamiltonian functional, and $\{, \}$ is the Poisson bracket, an antisymmetric, bilinear operator that obeys the Jacobi identity,

$$\{A, \{B, C\}\} + \{B, \{C, A\}\} + \{C, \{A, B\}\} = 0. \tag{1.2}$$

For example, the shallow-water equations

$$\frac{\partial u}{\partial t} = qhv - \Phi_x \tag{1.3a}$$

$$\frac{\partial v}{\partial t} = -qhu - \Phi_y \tag{1.3b}$$

$$\frac{\partial h}{\partial t} = -(hu)_x - (hv)_y \tag{1.3c}$$

fit the form (1.1) with

$$\begin{aligned} \{F, H\} = \iint d\mathbf{x} [q(F_u H_v - H_u F_v) - F_{\mathbf{u}} \cdot \nabla H_h \\ + H_{\mathbf{u}} \cdot \nabla F_h] \end{aligned} \tag{1.4}$$

and

$$H[u, v, h] = \frac{1}{2} \iint d\mathbf{x} (hu^2 + hv^2 + gh^2). \tag{1.5}$$

Here, (u, v) is the velocity in the (x, y) direction, h is the fluid depth,

$$q = (v_x - u_y + f)/h \tag{1.6}$$

is the potential vorticity, f is the Coriolis parameter, and

$$\Phi = \frac{1}{2} u^2 + \frac{1}{2} v^2 + gh. \tag{1.7}$$

We temporarily take f to be a constant, and the boundary conditions to be periodic; later we relax both assumptions. In (1.4) $F_u = \delta F / \delta u$ denotes the functional derivative of F with respect to u , and $F_{\mathbf{u}} = \delta F / \delta \mathbf{u} = (F_u, F_v)$. Since by (1.5)

Corresponding author address: Rick Salmon, Dept. 0213, 9500 Gilman Drive, UCSD, La Jolla, CA 92093-0213.
E-mail: rsalmon@ucsd.edu

$$\delta H = \iint d\mathbf{x} (hu\delta u + hv\delta v + \Phi\delta h), \quad (1.8)$$

we have $H_u = hu$ and $H_h = \Phi$. Let

$$F = u(\mathbf{x}_0) = \iint d\mathbf{x} u(\mathbf{x})\delta(\mathbf{x} - \mathbf{x}_0) \quad (1.9)$$

be the x -direction velocity at fixed location \mathbf{x}_0 . Then $F_u = \delta(\mathbf{x} - \mathbf{x}_0)$, $F_v = F_h = 0$, and (1.1) implies

$$\begin{aligned} \frac{d}{dt} u(\mathbf{x}_0) &= \{u(\mathbf{x}_0), H\} = \iint d\mathbf{x} (qH_v - \partial_x H_h)\delta(\mathbf{x} - \mathbf{x}_0) \\ &= (qh_v - \partial_x \Phi)|_{\mathbf{x}_0} \end{aligned} \quad (1.10)$$

in agreement with (1.3a). By similar steps we recover (1.3b) and (1.3c). For a general introduction to Hamiltonian fluid mechanics, see Shepherd (1990), Morrison (1998), or Salmon (1998).

Because the Poisson bracket is antisymmetric, the dynamics (1.1) conserve the energy,

$$\frac{dH}{dt} = \{H, H\} = 0. \quad (1.11)$$

This makes it very easy to construct numerical models that exactly conserve a discrete form of energy; one need only discretize the right-hand side of (1.1) in such a way that the antisymmetry property is maintained.¹

Nambu (1973) proposed a generalization of (1.1) in the form

$$\frac{dF}{dt} = \{F, H, Z\} \quad (1.12)$$

in which Z is an additional conserved quantity, besides the energy, and the Nambu bracket $\{F, H, Z\}$ is completely antisymmetric. Numerical models that retain the antisymmetry property of the Nambu bracket automatically conserve both H and Z . Since, as in the following example, (1.1) must result from the evaluation of Z in (1.12), it follows that Z is a Casimir of the Poisson bracket. That is, $\{F, Z\} = 0$ for any functional F .

The general Casimir of the shallow-water equations is

$$Z_G = \iint d\mathbf{x} hG(q), \quad (1.13)$$

where $G(q)$ is an arbitrary function of the potential vorticity q . In fact, shallow-water dynamics is equivalent to the Nambu-bracket formulation

$$\frac{dF}{dt} = \{F, H, Z_G\}_G, \quad (1.14)$$

where

$$\begin{aligned} \{F, H, Z_G\}_G &= \iint d\mathbf{x} \left\{ \frac{\delta(F, H)}{\delta(u, v)} \left(-\frac{1}{2G''q_x} \frac{\partial}{\partial x} \frac{\delta Z_G}{\delta h} - \frac{1}{2G''q_y} \frac{\partial}{\partial y} \frac{\delta Z_G}{\delta h} \right) \right. \\ &\quad \left. + \frac{1}{6(G - qG')} \left[J \left(\frac{\alpha(q)}{G''q_y} \frac{\delta F}{\delta u}, \frac{\alpha(q)}{G''q_y} \frac{\delta H}{\delta u} \right) + J \left(\frac{\alpha(q)}{G''q_x} \frac{\delta F}{\delta v}, \frac{\alpha(q)}{G''q_x} \frac{\delta H}{\delta v} \right) \right] \frac{\delta Z_G}{\delta h} + \text{cyc}(F, H, Z_G) \right\} \end{aligned} \quad (1.15)$$

is the Nambu bracket,

$$J(A, B) = \frac{\partial(A, B)}{\partial(x, y)}, \quad (1.16)$$

$$\alpha^2(q) = 6 \int dq G''(q)[qG'(q) - G(q)], \quad (1.17)$$

and $\text{cyc}(F, H, Z)$ denotes cyclic permutations of F , H , and Z . That is, substituting

$$\frac{\delta Z_G}{\delta u} = \partial_y G'(q), \quad \frac{\delta Z_G}{\delta v} = -\partial_x G'(q),$$

$$\frac{\delta Z_G}{\delta h} = G(q) - qG'(q) \quad (1.18)$$

into (1.15) yields (1.4) after tedious calculations. The bracket (1.15), which was discovered only after considerable effort and with the heavy use of symbolic manipulation software, is the only Nambu-bracket formulation of the shallow-water equations so far discovered that is formulated solely in terms of functional derivatives with respect to the basic variables u , v , and h . Discretizations of (1.5), (1.13), and (1.15) that maintain the antisymmetry property of (1.15) would automatically conserve the discrete analogs of H and Z_G . However, the complicated form of (1.15)—particularly the

¹ As in S05 we do not consider the error associated with the discretization of the left-hand side of (1.1). That is, we regard all time derivatives as exact. Experience shows that the truncation error associated with the time step is much less serious than the space-discretization error associated with approximations to the bracket.

appearance of q and its derivatives in denominators—poses special difficulties for the discretization of (1.15).

We therefore base the further developments of this paper on a simpler alternative to (1.15) that uses vorticity, divergence and depth as the dependent variables. We derive this bracket in section 2. In section 3, we use the Nambu bracket of section 2 to derive finite-difference analogs of the shallow-water equations that exactly conserve analogs of the energy, potential enstrophy, mass, and circulation on a regular square grid. In section 4 we compare solutions of the scheme derived in section 3 to previously known schemes with fewer conservation laws. Section 5 generalizes the Nambu-bracket scheme to nonperiodic domains, to higher-accuracy algorithms, and to a mesh composed of arbitrary triangles, including the regular hexagonal mesh as a special case. The results of section 5, which permit the construction of energy- and potential-enstrophy-conserving shallow-water algorithms on arbitrary curved surfaces with irregular boundaries, are the primary new results of the paper. Section 6 concludes.

S05 offered numerous examples to support the conjecture that every Hamiltonian fluid dynamics has a Nambu-bracket formulation corresponding to each of its Casimirs and, moreover, that the Nambu bracket corresponding to a particular Casimir is not unique. Thus it appears generally possible to construct numerical fluid models that automatically conserve analogs of the energy H and an arbitrary Casimir Z . In the simplest case of nonrotating, two-dimensional, incompressible flow (S05, sections 1–2), this method produces a generalization of Arakawa’s (1966) Jacobian that conserves the energy and an arbitrary moment $\iint d\mathbf{x} \zeta^n$ of the vorticity ζ . The enstrophy corresponds to $n = 2$. In two-dimensional flow, enstrophy conservation prevents the spurious transfer of energy into high wavenumbers, where it must eventually be removed by subgrid-scale viscosity. Numerical models of two-dimensional flow that in the inviscid limit conserve energy but not enstrophy must dissipate unrealistically large amounts of energy when eddy viscosity is added to the model, as is always necessary in practice. The same conclusion applies to shallow-water dynamics—see, for example, Sadourny (1975)—and, presumably, to the primitive equations as well. However, none of the primitive equation models now used to compute large-scale flow in the atmosphere and ocean conserve a form of energy and potential enstrophy in the inviscid limit. The eventual development of practical, global-scale, energy- and potential-enstrophy-conserving numerical models is a primary goal of the present work.

S05 presented a relatively wide range of examples, including the nonhydrostatic primitive equations. However, except in the case of two-dimensional incompressible flow, S05 stopped short of a complete derivation of the finite-difference equations, and no actual computations were shown. Thus S05 might disappoint applications-oriented readers unwilling to invest the effort required to fully work out all the formulae. In this paper, we focus solely on the shallow-water equations, and we derive the numerical equations in complete detail.

2. Nambu bracket for shallow-water dynamics

We begin by transforming the shallow-water Poisson bracket from old variables u, v, h to new variables ζ, μ, h , where $\zeta = v_x - u_y$ is the vorticity and $\mu = u_x + v_y$ is the divergence. Then (1.4) becomes

$$\{F, H\} = \{F, H\}_{\mu\mu} + \{F, H\}_{\zeta\zeta} + \{F, H\}_{\zeta\mu h}, \quad (2.1)$$

where

$$\{F, H\}_{\mu\mu} = \iint d\mathbf{x} qJ(F_\mu, H_\mu), \quad (2.2)$$

$$\{F, H\}_{\zeta\zeta} = \iint d\mathbf{x} qJ(F_\zeta, H_\zeta), \quad (2.3)$$

and

$$\begin{aligned} \{F, H\}_{\zeta\mu h} = \iint d\mathbf{x} [q(\nabla F_\mu \cdot \nabla H_\zeta - \nabla H_\mu \cdot \nabla F_\zeta) \\ + (\nabla F_\mu \cdot \nabla H_h - \nabla H_\mu \cdot \nabla F_h)]. \end{aligned} \quad (2.4)$$

As in section 1, $F_\mu = \delta F/\delta\mu$ denotes the functional derivative of F with respect to μ . To verify that (2.1) is equivalent to (1.4) we let

$$h\mathbf{u} = (-\chi_y + \gamma_x, \chi_x + \gamma_y). \quad (2.5)$$

Then [cf (1.8)]

$$\begin{aligned} \delta H &= \iint d\mathbf{x} [(-\chi_y + \gamma_x)\delta u + (\chi_x + \gamma_y)\delta v + \Phi\delta h] \\ &= \iint d\mathbf{x} [-\chi\delta(v_x - u_y) - \gamma\delta(u_x + v_y) + \Phi\delta h] \\ &= \iint d\mathbf{x} (-\chi\delta\zeta - \gamma\delta\mu + \Phi\delta h). \end{aligned} \quad (2.6)$$

It follows that

$$H_\zeta = -\chi, \quad H_\mu = -\gamma, \quad H_h = \Phi. \quad (2.7)$$

Letting $F = \zeta, \mu, h$ in (2.1), we obtain the evolution equations

$$\zeta_t = J(q, \chi) - \nabla \cdot (q \nabla \gamma) \quad (2.8a)$$

$$\mu_t = J(q, \gamma) + \nabla \cdot (q \nabla \chi - \nabla \Phi) \quad (2.8b)$$

$$h_t = -\nabla^2 \gamma. \quad (2.8c)$$

Combining (2.5) with the definitions of ζ and μ yields

$$\nabla \cdot (h^{-1} \nabla \chi) + J(h^{-1}, \gamma) = \zeta \quad (2.9a)$$

and

$$\nabla \cdot (h^{-1} \nabla \gamma) + J(\chi, h^{-1}) = \mu. \quad (2.9b)$$

It is straightforward to show that (2.8)–(2.9) are equivalent to (1.3) and the periodic boundary conditions; this proves the equivalence of (1.4) and (2.1).

Each of the brackets (2.2)–(2.4) is antisymmetric, and each has the same general Casimir (1.13) as (1.4). Here we are primarily interested in the mass

$$M = \iint d\mathbf{x} h, \quad (2.10) \quad \text{and}$$

the circulation,

$$C = \iint d\mathbf{x} h q = \iint d\mathbf{x} (\zeta + f), \quad (2.11)$$

and the potential enstrophy,

$$Z = \frac{1}{2} \iint d\mathbf{x} h q^2, \quad (2.12)$$

corresponding, respectively, to $G(q) = 1, q, \frac{1}{2}q^2$. As shown in S05, each of (2.2)–(2.4) has a Nambu-bracket formulation corresponding to Z . That is,

$$\{F, H\}_{\mu\mu} = \{F, H, Z\}_{\mu\mu\zeta} = \iint d\mathbf{x} J(F_\mu, H_\mu) Z_\zeta \quad (2.13)$$

$$\{F, H\}_{\zeta\zeta} = \{F, H, Z\}_{\zeta\zeta\zeta} = \iint d\mathbf{x} J(F_\zeta, H_\zeta) Z_\zeta \quad (2.14)$$

$$\begin{aligned} \{F, H\}_{\zeta\mu h} &= \{F, H, Z\}_{\zeta\mu h} \\ &= - \iint d\mathbf{x} (q_x)^{-1} [(\partial_x F_\mu \partial_x H_\zeta - \partial_x H_\mu \partial_x F_\zeta) \partial_x Z_h + \text{cyc}(F, H, Z)] \\ &\quad - \iint d\mathbf{x} (q_y)^{-1} [(\partial_y F_\mu \partial_y H_\zeta - \partial_y H_\mu \partial_y F_\zeta) \partial_y Z_h + \text{cyc}(F, H, Z)]. \end{aligned} \quad (2.15)$$

None of (2.13)–(2.15) is unique, and their sum is not equivalent to (1.15) (with $Z_G = Z$) for arbitrary F, H, Z .² However, substituting

$$Z_\zeta = q, \quad Z_\mu = 0, \quad Z_h = -\frac{1}{2}q^2 \quad (2.16)$$

into (2.13)–(2.15) yields (2.2)–(2.4). In carrying out these substitutions, we find that the functional derivatives (2.16) cancel the apparent singularities in (2.15)—the denominators containing q_x and q_y . This is of course expected; the shallow-water equations contain no singularities.

We obtain numerical analogs of the shallow-water equations that automatically conserve H and Z by re-

placing (2.13)–(2.15) with finite-difference approximations that maintain the antisymmetry properties of (2.13)–(2.15). However, unless the finite-difference approximations also maintain the property that the apparent singularities in (2.15) are cancelled by the functional derivatives of Z , the model will contain artificial singularities.

3. Regular square grid

We consider a periodic square grid with grid spacing Δ , and all the variables defined at every grid point. We let

$$Z = \frac{1}{2} \sum_{ij} h_{ij} q_{ij}^2 = \frac{1}{2} \sum_{ij} \frac{(\zeta_{ij} + f_{ij})^2}{h_{ij}} \quad (3.1)$$

be the discrete analog of (2.12), where h_{ij} denotes the value at grid point ij . Since (3.1) does not depend on μ_{ij} , (2.2) conserves Z automatically; we do not actually need to use (2.13). The discretization

² Every term in (1.15) contains a functional derivative with respect to h , whereas (2.13) and (2.14) do not. Thus the Nambu brackets (1.15) and (2.13)–(2.15) are not equivalent even though they correspond to equivalent Poisson brackets.

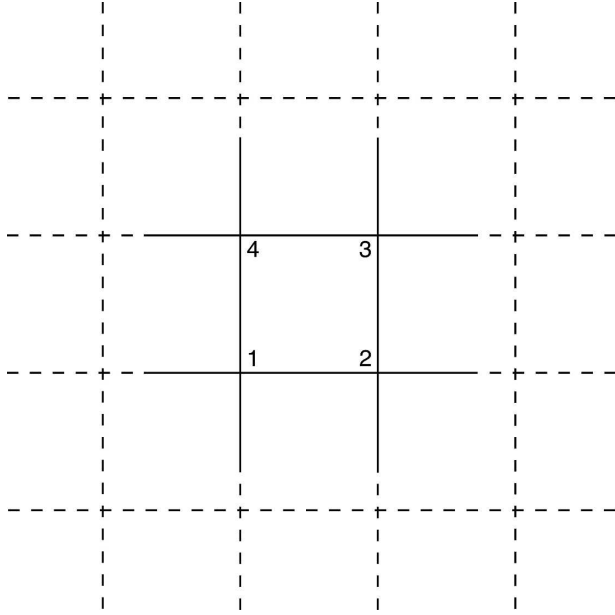


FIG. 1. A single grid box with corners numbered as in the text.

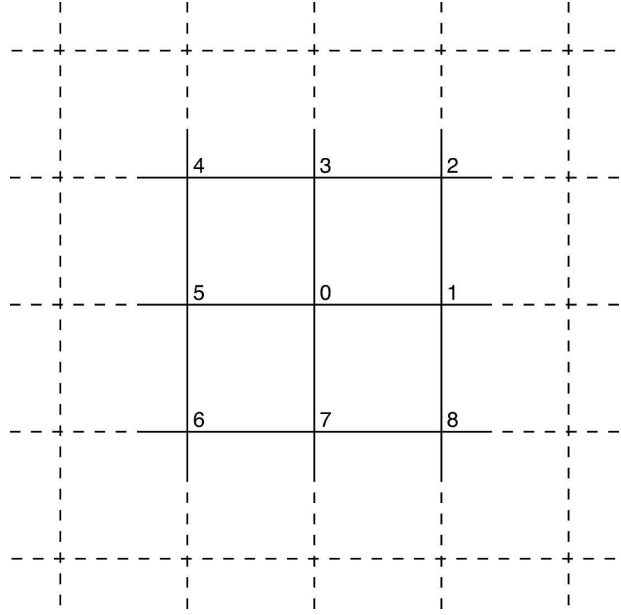


FIG. 2. An arbitrary grid point, labeled 0, and its neighbors.

$$\begin{aligned}
 \iint d\mathbf{x} qJ(F_\mu, H_\mu) &\rightarrow \frac{1}{2\Delta^2} \sum_{\text{grid boxes}} \frac{1}{4} (q_1 + q_2 + q_3 + q_4) \\
 &\times \left[\left(\frac{\partial F}{\partial \mu_3} - \frac{\partial F}{\partial \mu_1} \right) \left(\frac{\partial H}{\partial \mu_4} - \frac{\partial H}{\partial \mu_2} \right) - \left(\frac{\partial H}{\partial \mu_3} - \frac{\partial H}{\partial \mu_1} \right) \left(\frac{\partial F}{\partial \mu_4} - \frac{\partial F}{\partial \mu_2} \right) \right] \\
 &= \frac{1}{2\Delta^2} \sum_{\text{grid boxes}} q_{1234} \left\{ \frac{\partial(F, H)}{\partial(\mu_1, \mu_2)} + \frac{\partial(F, H)}{\partial(\mu_2, \mu_3)} + \frac{\partial(F, H)}{\partial(\mu_3, \mu_4)} + \frac{\partial(F, H)}{\partial(\mu_4, \mu_1)} \right\} \quad (3.2)
 \end{aligned}$$

maintains the antisymmetry with respect to F and H , and hence maintains the conservation of H . In (3.2) the summation is over all the grid boxes on the periodic plane,

$$q_{1234} = \frac{1}{4} (q_1 + q_2 + q_3 + q_4), \quad (3.3)$$

and the integer subscripts refer to the corners of each local grid box as shown on Fig. 1. In (2.8), (3.2) contributes only the Jacobian term in (2.8b). Thus, setting $F = \mu_0$, where the zero subscript corresponds to the arbitrary grid point at the center of Fig. 2, and defining

$$\gamma_i = -\partial H / \partial \mu_i, \quad \chi_i = -\partial H / \partial \zeta_i, \quad \Phi_i = \partial H / \partial h_i \quad (3.4)$$

[cf (2.7)], we obtain

$$\begin{aligned}
 \frac{d\mu_0}{dt} &= \frac{1}{2\Delta^2} \{ q_{0123}(\gamma_3 - \gamma_1) + q_{0345}(\gamma_5 - \gamma_3) \\
 &+ q_{0567}(\gamma_7 - \gamma_5) + q_{0781}(\gamma_1 - \gamma_7) \} + \dots \quad (3.5)
 \end{aligned}$$

as the approximation to the Jacobian term in (2.8b). The four terms in (3.5) represent the contributions from the four grid boxes surrounding point 0 in Fig. 2. The Hamiltonian remains unspecified. That is, the dependence of H on ζ_i, μ_i, h_i remains to be defined. However, (3.5) conserves any H with derivatives defined by (3.4).

For (2.3), we must use the corresponding Nambu bracket (2.14). To ensure that the discrete approximation is completely antisymmetric, we first rewrite (2.14) as

$$\{F, H, Z\}_{\zeta\zeta\zeta} = \frac{1}{3} \iint d\mathbf{x} [J(F_\zeta, H_\zeta)Z_\zeta + \text{cyc}(F, H, Z)]. \quad (3.6)$$

Then we replace each of the three Jacobian terms in (3.6) by finite-difference approximations of the form

$$\int \int dx J(F_{\zeta}, H_{\zeta}) Z_{\zeta} \rightarrow \sum_{\text{grid boxes}} \frac{1}{4} \left(\frac{\partial Z}{\partial \zeta_1} + \frac{\partial Z}{\partial \zeta_2} + \frac{\partial Z}{\partial \zeta_3} + \frac{\partial Z}{\partial \zeta_4} \right) \times \frac{1}{2\Delta^2} \left[\left(\frac{\partial F}{\partial \zeta_3} - \frac{\partial F}{\partial \zeta_1} \right) \left(\frac{\partial H}{\partial \zeta_4} - \frac{\partial H}{\partial \zeta_2} \right) - \left(\frac{\partial H}{\partial \zeta_3} - \frac{\partial H}{\partial \zeta_1} \right) \left(\frac{\partial F}{\partial \zeta_4} - \frac{\partial F}{\partial \zeta_2} \right) \right] \tag{3.7}$$

where, once again, the subscripts refer to Fig. 1. Collecting terms, we obtain the approximation

$$\{F, H, Z\}_{\zeta\zeta\zeta} = \frac{1}{12\Delta^2} \sum_{\text{grid boxes}} \left[\frac{\partial(F, H, Z)}{\partial(\zeta_1, \zeta_2, \zeta_3)} + \frac{\partial(F, H, Z)}{\partial(\zeta_1, \zeta_2, \zeta_4)} + \frac{\partial(F, H, Z)}{\partial(\zeta_1, \zeta_3, \zeta_4)} + \frac{\partial(F, H, Z)}{\partial(\zeta_2, \zeta_3, \zeta_4)} \right] \tag{3.8}$$

to (2.14). The discrete Nambu bracket (3.8) conserves H and Z by its manifest antisymmetry with respect to F, H , and Z . In (2.8), the Nambu bracket (3.8) only contributes the Jacobian term in (2.8a). Setting $F = \zeta_0$, and using (3.1) and (3.4), we obtain the approximation

$$\frac{d\zeta_0}{dt} = \frac{1}{12\Delta^2} [(\chi_2 + \chi_3 - \chi_7 - \chi_8)q_1 + (\chi_3 - \chi_1)q_2 + (\chi_4 + \chi_5 - \chi_1 - \chi_2)q_3 + (\chi_5 - \chi_3)q_4 + (\chi_6 + \chi_7 - \chi_3 - \chi_4)q_5 + (\chi_7 - \chi_5)q_6 + (\chi_8 + \chi_1 - \chi_5 - \chi_6)q_7 + (\chi_1 - \chi_7)q_8] + \dots \tag{3.9}$$

to the Jacobian term in (2.8a), where the subscripts refer to Fig. 2. The approximation (3.9) is in fact Arakawa's (1966) second-order Jacobian; see also Salmon and Talley (1989).

The remaining, non-Jacobian terms in (2.8) correspond to the Nambu bracket (2.15). We replace (2.15) by

$$\{F, H, Z\}_{\zeta\mu h} = -\frac{1}{\Delta^2} \sum_{\text{grid boxes}} \left\{ \frac{1}{(q_2 - q_1)} \left[\left(\frac{\partial F}{\partial \mu_2} - \frac{\partial F}{\partial \mu_1} \right) \left(\frac{\partial H}{\partial \zeta_2} - \frac{\partial H}{\partial \zeta_1} \right) - \left(\frac{\partial H}{\partial \mu_2} - \frac{\partial H}{\partial \mu_1} \right) \left(\frac{\partial F}{\partial \zeta_2} - \frac{\partial F}{\partial \zeta_1} \right) \right] \left(\frac{\partial Z}{\partial h_2} - \frac{\partial Z}{\partial h_1} \right) + \frac{1}{(q_4 - q_1)} \left[\left(\frac{\partial F}{\partial \mu_4} - \frac{\partial F}{\partial \mu_1} \right) \left(\frac{\partial H}{\partial \zeta_4} - \frac{\partial H}{\partial \zeta_1} \right) - \left(\frac{\partial H}{\partial \mu_4} - \frac{\partial H}{\partial \mu_1} \right) \left(\frac{\partial F}{\partial \zeta_4} - \frac{\partial F}{\partial \zeta_1} \right) \right] \left(\frac{\partial Z}{\partial h_4} - \frac{\partial Z}{\partial h_1} \right) + \text{cyc}(F, H, Z) \right\} = -\frac{1}{\Delta^2} \sum_{\text{grid boxes}} \left\{ \frac{1}{(q_2 - q_1)} \left[\frac{\partial(F, H, Z)}{\partial(\mu_2, \zeta_2, h_2)} - \frac{\partial(F, H, Z)}{\partial(\mu_1, \zeta_2, h_2)} - \frac{\partial(F, H, Z)}{\partial(\mu_2, \zeta_1, h_2)} + \frac{\partial(F, H, Z)}{\partial(\mu_1, \zeta_1, h_2)} - \frac{\partial(F, H, Z)}{\partial(\mu_2, \zeta_2, h_1)} + \frac{\partial(F, H, Z)}{\partial(\mu_1, \zeta_2, h_1)} + \frac{\partial(F, H, Z)}{\partial(\mu_2, \zeta_1, h_1)} - \frac{\partial(F, H, Z)}{\partial(\mu_1, \zeta_1, h_1)} \right] + \frac{1}{(q_4 - q_1)} \left[\frac{\partial(F, H, Z)}{\partial(\mu_4, \zeta_4, h_4)} - \frac{\partial(F, H, Z)}{\partial(\mu_1, \zeta_4, h_4)} - \frac{\partial(F, H, Z)}{\partial(\mu_4, \zeta_1, h_4)} + \frac{\partial(F, H, Z)}{\partial(\mu_1, \zeta_1, h_4)} - \frac{\partial(F, H, Z)}{\partial(\mu_4, \zeta_4, h_1)} + \frac{\partial(F, H, Z)}{\partial(\mu_1, \zeta_4, h_1)} + \frac{\partial(F, H, Z)}{\partial(\mu_4, \zeta_1, h_1)} - \frac{\partial(F, H, Z)}{\partial(\mu_1, \zeta_1, h_1)} \right] \right\}, \tag{3.10}$$

where the subscripts refer to Fig. 1. Then, setting $F = \zeta_0, \mu_0, h_0$, we obtain the following replacements for the remaining terms in (2.8):

$$-\nabla \cdot (q\nabla\gamma) \rightarrow \frac{1}{2\Delta^2} [(\gamma_0 - \gamma_1)(q_0 + q_1) + (\gamma_0 - \gamma_3)(q_0 + q_3) + (\gamma_0 - \gamma_5)(q_0 + q_5) + (\gamma_0 - \gamma_7)(q_0 + q_7)] \tag{3.11}$$

$$\nabla \cdot (q\nabla\chi) \rightarrow -\frac{1}{2\Delta^2} [(\chi_0 - \chi_1)(q_0 + q_1) + (\chi_0 - \chi_3)(q_0 + q_3) + (\chi_0 - \chi_5)(q_0 + q_5) + (\chi_0 - \chi_7)(q_0 + q_7)] \tag{3.12}$$

$$-\nabla^2\Phi \rightarrow \Delta^{-2}(4\Phi_0 - \Phi_1 - \Phi_3 - \Phi_5 - \Phi_7) \tag{3.13}$$

$$-\nabla^2\gamma \rightarrow \Delta^{-2}(4\gamma_0 - \gamma_1 - \gamma_3 - \gamma_5 - \gamma_7), \tag{3.14}$$

where the subscripts refer to Fig. 2. In summary, the equations

$$\frac{d\zeta_0}{dt} = (3.9) + (3.11) \tag{3.15a}$$

$$\frac{d\mu_0}{dt} = (3.5) + (3.12) + (3.13) \tag{3.15b}$$

$$\frac{dh_0}{dt} = (3.14) \tag{3.15c}$$

represent a finite-difference approximation to (2.8) that conserves (3.1) and arbitrary energy H , with derivatives (3.4). By inspection, (3.15) also conserves the mass (2.10) and the circulation (2.11). Although the circulation vanishes identically in the case of periodic boundary conditions, the existence of a local, flux-form conservation law for ζ is significant. In the limiting case of two-dimensional, incompressible flow with constant f , the conservation of $\iint d\mathbf{x} (\zeta + f)^2$ implies conservation of $\iint d\mathbf{x} \zeta^2$ only if $\iint d\mathbf{x} \zeta$ is also conserved.

The approximations (3.2), (3.8), and (3.10) are probably the simplest finite-difference approximations that maintain the antisymmetry properties of (2.13)–(2.15). The evolution Eqs. (3.15) are correspondingly simple.

Other, more accurate, approximations are possible; it only matters that the antisymmetry be maintained. The approximations need not even be finite-difference approximations; they could be a mixture of finite differences, finite elements, and spectral modes. Moreover, the methods by which we approximate each of (2.13), (2.14), and (2.15) are completely independent. This gives the method great flexibility. In section 5 we use this flexibility to develop an approximation method that applies to an unstructured triangular mesh, and hence to any mesh composed of polygons that can be decomposed into triangles. First, however, we complete our derivation on the square grid.

It remains to approximate the energy H . Once again, the manner in which we discretize H is completely independent from the discrete evolution Eqs. (3.15). Combining (1.5) and (2.5), we have

$$H = \iint d\mathbf{x} \left\{ \frac{1}{2h} [\nabla\chi \cdot \nabla\chi + \nabla\gamma \cdot \nabla\gamma + 2J(\chi, \gamma)] + \frac{1}{2} gh^2 \right\}. \tag{3.16}$$

We replace

$$H \rightarrow \Delta^{-2} \sum_{\text{grid boxes}} \{[(\chi_2 - \chi_1)^2 + (\gamma_2 - \gamma_1)^2](h_1 + h_2)^{-1} + [(\chi_4 - \chi_1)^2 + (\gamma_4 - \gamma_1)^2](h_1 + h_4)^{-1} + 2[(\chi_3 - \chi_1)(\gamma_4 - \gamma_2) - (\gamma_3 - \gamma_1)(\chi_4 - \chi_2)](h_1 + h_2 + h_3 + h_4)^{-1}\} + \frac{1}{2} \sum_{ij} gh_{ij}^2 \tag{3.17}$$

where, once again, the integer subscripts refer to Fig. 1. Then, by direct manipulations,

$$dH = \sum_{ij} (-\chi_{ij} d\zeta_{ij} - \gamma_{ij} d\mu_{ij} + \Phi_{ij} dh_{ij}), \tag{3.18}$$

where, in the notation of Fig. 2,

$$\zeta_0 = \frac{2}{\Delta^2} \left[\frac{\chi_1}{h_0 + h_1} + \frac{\chi_3}{h_0 + h_3} + \frac{\chi_5}{h_0 + h_5} + \frac{\chi_7}{h_0 + h_7} - \left(\frac{1}{h_0 + h_1} + \frac{1}{h_0 + h_3} + \frac{1}{h_0 + h_5} + \frac{1}{h_0 + h_7} \right) \chi_0 + \frac{(\gamma_3 - \gamma_1)}{(h_0 + h_1 + h_2 + h_3)} + \frac{(\gamma_5 - \gamma_3)}{(h_0 + h_3 + h_4 + h_5)} + \frac{(\gamma_7 - \gamma_5)}{(h_0 + h_5 + h_6 + h_7)} + \frac{(\gamma_1 - \gamma_7)}{(h_0 + h_7 + h_8 + h_1)} \right], \tag{3.19a}$$

$$\mu_0 = \frac{2}{\Delta^2} \left[\frac{\gamma_1}{h_0 + h_1} + \frac{\gamma_3}{h_0 + h_3} + \frac{\gamma_5}{h_0 + h_5} + \frac{\gamma_7}{h_0 + h_7} - \left(\frac{1}{h_0 + h_1} + \frac{1}{h_0 + h_3} + \frac{1}{h_0 + h_5} + \frac{1}{h_0 + h_7} \right) \gamma_0 - \frac{(\chi_3 - \chi_1)}{(h_0 + h_1 + h_2 + h_3)} - \frac{(\chi_5 - \chi_3)}{(h_0 + h_3 + h_4 + h_5)} - \frac{(\chi_7 - \chi_5)}{(h_0 + h_5 + h_6 + h_7)} - \frac{(\chi_1 - \chi_7)}{(h_0 + h_7 + h_8 + h_1)} \right], \tag{3.19b}$$

and

$$\begin{aligned} \Phi_0 = gh_0 + \frac{1}{\Delta^2} \left\{ & [(\chi_1 - \chi_0)^2 + (\gamma_1 - \gamma_0)^2](h_0 + h_1)^{-2} + [(\chi_3 - \chi_0)^2 + (\gamma_3 - \gamma_0)^2](h_0 + h_3)^{-2} + [(\chi_5 - \chi_0)^2 + (\gamma_5 - \gamma_0)^2](h_0 + h_5)^{-2} \right. \\ & + [(\chi_7 - \chi_0)^2 + (\gamma_7 - \gamma_0)^2](h_0 + h_7)^{-2} + \frac{2[(\chi_2 - \chi_0)(\gamma_3 - \gamma_1) - (\gamma_2 - \gamma_0)(\chi_3 - \chi_1)]}{(h_0 + h_1 + h_2 + h_3)^2} \\ & + \frac{2[(\chi_1 - \chi_7)(\gamma_0 - \gamma_8) - (\gamma_1 - \gamma_7)(\chi_0 - \chi_8)]}{(h_0 + h_7 + h_8 + h_1)^2} + \frac{2[(\chi_3 - \chi_5)(\gamma_4 - \gamma_0) - (\gamma_3 - \gamma_5)(\chi_4 - \chi_0)]}{(h_0 + h_3 + h_4 + h_5)^2} \\ & \left. + \frac{2[(\chi_0 - \chi_6)(\gamma_5 - \gamma_7) - (\gamma_0 - \gamma_6)(\chi_5 - \chi_7)]}{(h_0 + h_5 + h_6 + h_7)^2} \right\}. \end{aligned} \quad (3.20)$$

Equations (3.19) are analogous to (2.9); (3.20) is a finite-difference approximation to (1.7) and (2.5). The forms of (3.19) and (3.20) are completely determined by the choice (3.17) of approximate Hamiltonian. This choice is arbitrary except that it must lead to invertible elliptic, finite-difference operators in the Eqs. (3.19) for χ and γ . If these elliptic operators had turned out to be singular—that is, if their spectrum contained a zero eigenvalue—then the finite-difference equations would acquire a computational mode. The choice (3.17) was guided by a desire that the operators in (3.19) reduce to the standard (and nonsingular) five-point difference formula for the Laplacian in the case of uniform h . It is interesting that our formulation requires no precise definition of u and v in terms of χ and γ . Although we may infer a relationship between these variables from (3.17), the velocity components do not appear in the model equations.

The complete shallow-water model comprises (3.15), (3.19), and (3.20). We use (3.15) to step the variables ζ , μ , h forward in time. Then we find χ and γ at the new time by solving the coupled elliptic Eqs. (3.19) subject to the periodic boundary conditions. Then (3.20) gives Φ at the new time, and the process repeats. The dynamics (3.15), (3.19)–(3.20) conserves the energy (3.17), the potential enstrophy (3.1), and by inspection of (3.15) finite-difference approximations to the mass (2.10) and circulation (2.11).

4. Numerical tests and comparisons

In this section we compare the shallow-water model derived in the previous section (hereafter called NB, for *Nambu*) to four alternatives. The first of these, NBE (*Nambu*, conserving only energy), is identical to NB except that the Jacobian (3.9) in (3.15a) is replaced by the Jacobian (3.5) [with the γ 's in (3.5) replaced by χ 's; see (2.8)]. This single, minor modification of NB destroys its conservation of potential enstrophy. The re-

maining three comparison schemes are C-grid schemes in which the fundamental variables are u , v , and h . These C-grid schemes do not require the solution of elliptic equations like (3.19), hence they can be solved much more efficiently than NB. The C-grid schemes include: SE, the scheme of Sadourny [1975, Eq. (3)], which conserves energy but not potential enstrophy; SZ [Sadourny 1975, Eq. (4)], which conserves potential enstrophy but not energy; and AL, the energy- and potential-enstrophy-conserving scheme of Arakawa and Lamb (1981). All five schemes conserve the mass (2.10) and the circulation (2.11).

In the linear (small-amplitude) limit, the behavior of each scheme is well summarized by its dispersion relationship for inertia-gravity waves. In this limit, NB (and NBE) reduce to the Z-grid equations analyzed by Randall (1994). The corresponding dispersion relationship is

$$\omega^2 = f^2 + 4gH_0\Delta^{-2}[\sin^2(k\Delta/2) + \sin^2(l\Delta/2)], \quad (4.1)$$

where ω is the frequency, (k, l) the wavenumber, and H_0 the mean depth. On the other hand, the C-grid schemes (SE, SZ, and AL) correspond to

$$\begin{aligned} \omega^2 = \frac{1}{4}f^2[1 + \cos(k\Delta) + \cos(l\Delta) + \cos(k\Delta)\cos(l\Delta)] \\ + 4gH_0\Delta^{-2}[\sin^2(k\Delta/2) + \sin^2(l\Delta/2)]. \end{aligned} \quad (4.2)$$

In the limit of perfect resolution ($k\Delta, l\Delta \rightarrow 0$), both (4.1) and (4.2) correctly limit on the exact dispersion relation,

$$\omega^2 = f^2 + gH_0(k^2 + l^2). \quad (4.3)$$

However, for poorly resolved waves with $k\Delta, l\Delta \rightarrow \pi$, the Coriolis term in (4.2) actually disappears. Randall (1994), building on the work of Arakawa and Lamb (1977), notes that (4.1), like (4.3), increases monotonically with wavenumber at all resolved wavenumbers, whereas (4.2) grossly misrepresents (4.3) when $\sqrt{gH_0}/f < \Delta$.

It follows that the C-grid schemes do not correctly simulate geostrophic adjustment in cases in which the deformation radius is poorly resolved. Of course, all atmospheric models and most oceanographic models resolve the first internal deformation radius. But if we regard the shallow-water equations as a paradigm for an arbitrary vertical mode of the primitive equations, for which the deformation radius of mode n scales as n^{-1} , then we must conclude that the C-grid schemes do not accurately simulate geostrophic adjustment in any but the lowest vertical modes.

The inaccurate Coriolis term in (4.2) results from the unavoidable staggering of variables on the C-grid. Salmon (2004) conducted an exhaustive search for energy- and potential-entrophy-conserving schemes corresponding to the conventional, u - v - h , form of the shallow-water equations. In all the schemes found, the Coriolis force is computed as an average over many grid points. The simplest of the schemes found by Salmon (2004) are C-grid schemes, and AL is the simplest of these. Thus it seems that all doubly conservative schemes based upon the u - v - h form of the shallow-water equations incorrectly simulate geostrophic adjustment. In this respect NB is superior to AL. This advantage of NB at least partly offsets the disadvantage of solving elliptic equations.

Now we consider fully nonlinear, shallow-water solutions in a $2\pi \times 2\pi$ periodic box. In all schemes, we step forward in time using the third-order Adams–Bashforth method (Durran 1991). In the Nambu schemes, we solve (3.19) with an iterative multigrid solver.

To demonstrate the importance of conserving potential entrophy, we first consider inviscid, nonrotating ($f = 0$) solutions of NB and NBE that begin from the same random initial conditions, with a Froude number $U_{\text{rms}}(gh_{\text{avg}})^{-1/2}$ of 0.1. Recall that NB and NBE differ only in the finite-difference form of a single term in a single equation. Hence it seems fair to attribute the differences in the two solutions to the lack of potential entrophy conservation in NBE. Since viscosity is absent, both solutions gradually cease to be smooth, but the nonconservation of potential entrophy in NBE allows significant energy to reach the highest resolved wavenumbers. Figure 3 shows the common initial entrophy spectrum, and the spectrum in NB and NBE at a later time in which the entrophy cascade is fully developed. (This time, which corresponds to 40 000 time steps, is the time required for fluid particles to travel 1.6 times the periodic box size at the rms velocity.) At the time of Fig. 3, the energy in both experiments is within 0.5% of its initial value. This small error is mainly the result of incomplete convergence in the multigrid

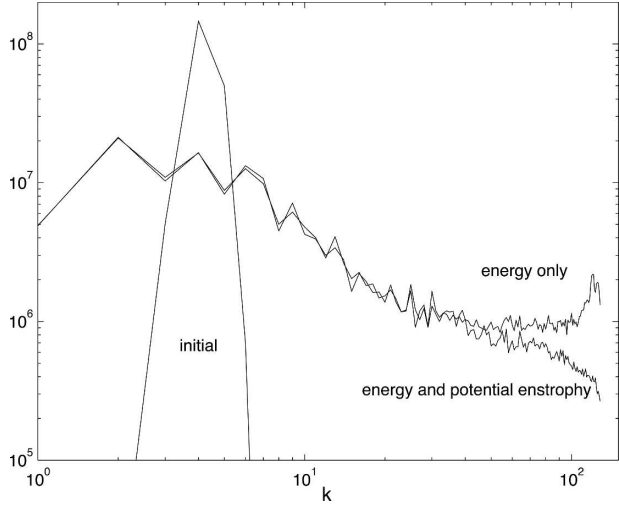


FIG. 3. The initial entrophy spectrum and the entrophy spectra at a later time in two inviscid solutions of the shallow-water equations that begin from the same random initial conditions. One of the solutions, NB, conserves energy and potential entrophy, while the other solution, NBE, conserves only the energy.

solver, because the potential entrophy in NB (which is affected only by the truncation error in the time step) is within 0.000 11% of its initial value. In contrast, the potential entrophy in NBE has increased by nearly 26%. Similar experiments with the C-grid schemes show that SE, like NBE, exhibits a spurious transfer of energy to high wavenumber, compared to the potential-entrophy-conserving schemes SZ, AL, and NB.

None of the schemes conserves the potential vorticity moments

$$Z_n = \iint d\mathbf{x} hq^n \quad (4.4)$$

for $n > 2$. However, numerical experiments show that the potential-entrophy conserving schemes also do a better job of conserving the higher moments of the potential vorticity than do NBE and SE. Figure 4, which is typical, shows time series of the ratio of Z_6 to its initial value in NB and in the three C-grid schemes, beginning from the same random initial conditions as in the previously described experiment. At the time of Fig. 4, the potential entrophy in SE has increased by about 30% over its initial value. However, Z_6 has grown to more than 5 times its initial value, and is about twice as large as in the three potential entrophy–conserving schemes. This and many similar results offer strong indirect evidence that potential entrophy–conserving schemes do a better job of conserving potential vorticity on particles than do SE and NBE.

However, the experiments also suggest that SZ, while

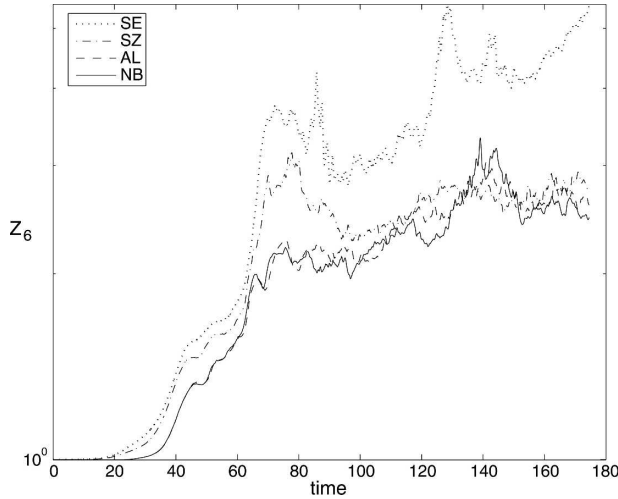


FIG. 4. Time series of Z_6 , defined by (4.4), the sixth moment of potential enstrophy, divided by its initial value, in four inviscid solutions of the shallow-water equations that begin from the same random initial conditions. Solution SE conserves energy but not the potential enstrophy Z_2 ; the other three solutions conserve potential enstrophy.

much better than SE, is at least slightly inferior to the doubly conservative schemes AL and NB. Figure 5 shows the potential vorticity in NB and in the three C-grid schemes for an inviscid, nonrotating experiment that began with sinusoidally perturbed shear layers. With no viscosity present, all of the solutions eventually exhibit oscillations on the scale of the grid spacing. However, the oscillations in SZ are much larger than in AL and NB, and are nearly as bad as in SE. In this and other experiments, the close agreement between NB and AL is striking, particularly considering the huge differences in the way the two schemes are constructed. This supports the idea that conservation laws are important determinants of overall behavior.

Next we compare rotating ($f \neq 0$) solutions in which a Navier–Stokes friction of the form

$$\frac{\partial u_i}{\partial t} = \dots + \frac{\nu}{h} \frac{\partial}{\partial x_j} \left(\frac{\partial u_i}{\partial x_j} + \frac{\partial u_j}{\partial x_i} \right), \quad (4.5)$$

is appended to the momentum equations (with corresponding terms appended to the equations for vorticity and divergence). In units for which $g = h_{\text{avg}} = 1$, we set $f = 1$, corresponding to a deformation radius of unity. Once again, the periodic box size is 2π . Thus the deformation radius is well-resolved, and the C-grid schemes therefore suffer no disadvantage in their ability to simulate inertia–gravity waves. The common initial condition is

$$h(x, y) = 1 + 0.1[H(1 - r_1) + H(1 - r_2)], \quad (4.6)$$

where $H()$ is a smooth approximation to the Heaviside function, and r_1, r_2 are the distances between (x, y) and the points $(-1, 0)$, $(1, 0)$ respectively. Thus (4.6) corresponds to a dumbbell-shaped pattern of surface elevation. The initial velocity field is in geostrophic balance with (4.6) and corresponds to $U_{\text{rms}} \sim 0.1$. Hence the Froude number and the Rossby number based upon the deformation radius are both of order 0.1. The constant viscosity coefficient $\nu = .0002$. Figure 6 shows the potential vorticity fields in solutions of NB and in solutions of the three C-grid schemes at the later time $t = 12$. All four solutions have the same resolution for all dependent variables (whether staggered or not), corresponding to 256×256 grid points. Figure 7 shows the potential vorticity at the same time in four corresponding solutions with a higher resolution of 512×512 grid points. In this and many similar experiments, the solutions of the doubly conservative schemes AL and NB are more accurate, and resemble those of the singly conservative schemes SE and SZ at twice the spatial resolution. Figure 8 shows the enstrophy spectra in the solutions corresponding to Fig. 7. The spectrum corresponding to SE shows the expected excess of enstrophy at high wavenumber, but in this case the excess in SZ is even greater. The spectra of AL and NB contain significantly less enstrophy at high wavenumber, and moreover are nearly identical.

In summary, the simultaneous conservation of energy and potential enstrophy in NB and AL prevents the spurious turbulent cascade of energy to high wavenumbers, as expected. In this respect, SE performs very poorly, while SZ does about as well as NB and AL. However, careful comparisons of particular, highly structured solutions—viscous and inviscid, rotating and nonrotating—have shown that NB and AL are significantly more accurate than the other schemes, and usually yield nearly identical results. The agreement between AL and NB is remarkable, considering the huge differences in the way the two schemes are constructed, and it suggests that the conservation laws are important determinants of overall behavior. However, in cases in which the deformation radius is poorly resolved, linear waves analysis shows that NB is superior to AL.

Nevertheless, we make no claim that NB is better than any of the previously discovered energy- and potential-enstrophy-conserving models, including those of Arakawa and Lamb (1981), Abramopoulos (1988), Ringler and Randall (2002), and Salmon (2004). Rather, the significance of the present contribution lies in the generality and flexibility of the method used to derive (3.15). As demonstrated in the following section,

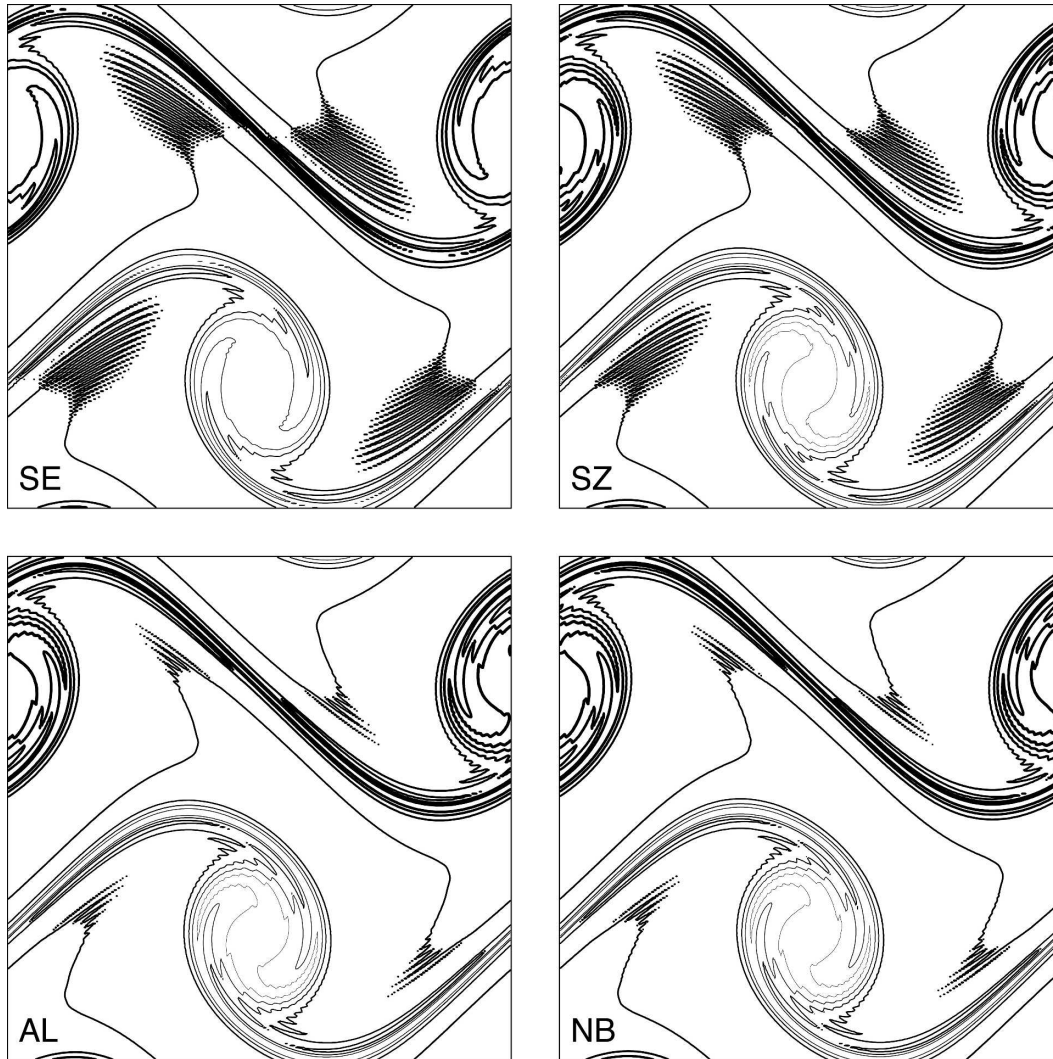


FIG. 5. The potential vorticity field at the same time in four numerical solutions of the inviscid shallow-water equations that began from the same initial conditions; the solutions AL and NB, which conserve both energy and potential enstrophy, exhibit fewer small-scale oscillations than SE, which conserves only energy, and SZ, which conserves only potential enstrophy.

this permits significant generalizations, including the generalization to an arbitrary unstructured grid of polygons.

5. Generalizations

Our derivation has made frequent use of the periodic boundary conditions. However, the brackets (2.13)–(2.15) remain valid if the periodic boundary conditions are replaced by solid walls at which χ and the normal derivative of γ vanish. By (2.5) this corresponds to boundary conditions of no normal flow. These new boundary conditions replace the periodic boundary conditions on (2.9). All of this carries over to the finite-

difference approximations. The discrete evolution Eqs. (3.15) are unchanged at interior grid points, but at boundary points the right-hand sides of (3.15) lose the terms arising from grid boxes that lie outside the boundaries. Equations (3.19) and (3.20) are unchanged except for the new boundary conditions on (3.19). When boundaries are present, the Coriolis parameter can depend arbitrarily on location. All the conservation laws remain intact.

The model based on (3.15), (3.19)–(3.20) has second-order accuracy in the grid spacing. To achieve higher accuracy, we need only replace (3.2), (3.8), (3.10), and (3.17) by finite-difference approximations of higher accuracy. For the case of periodic boundary conditions,

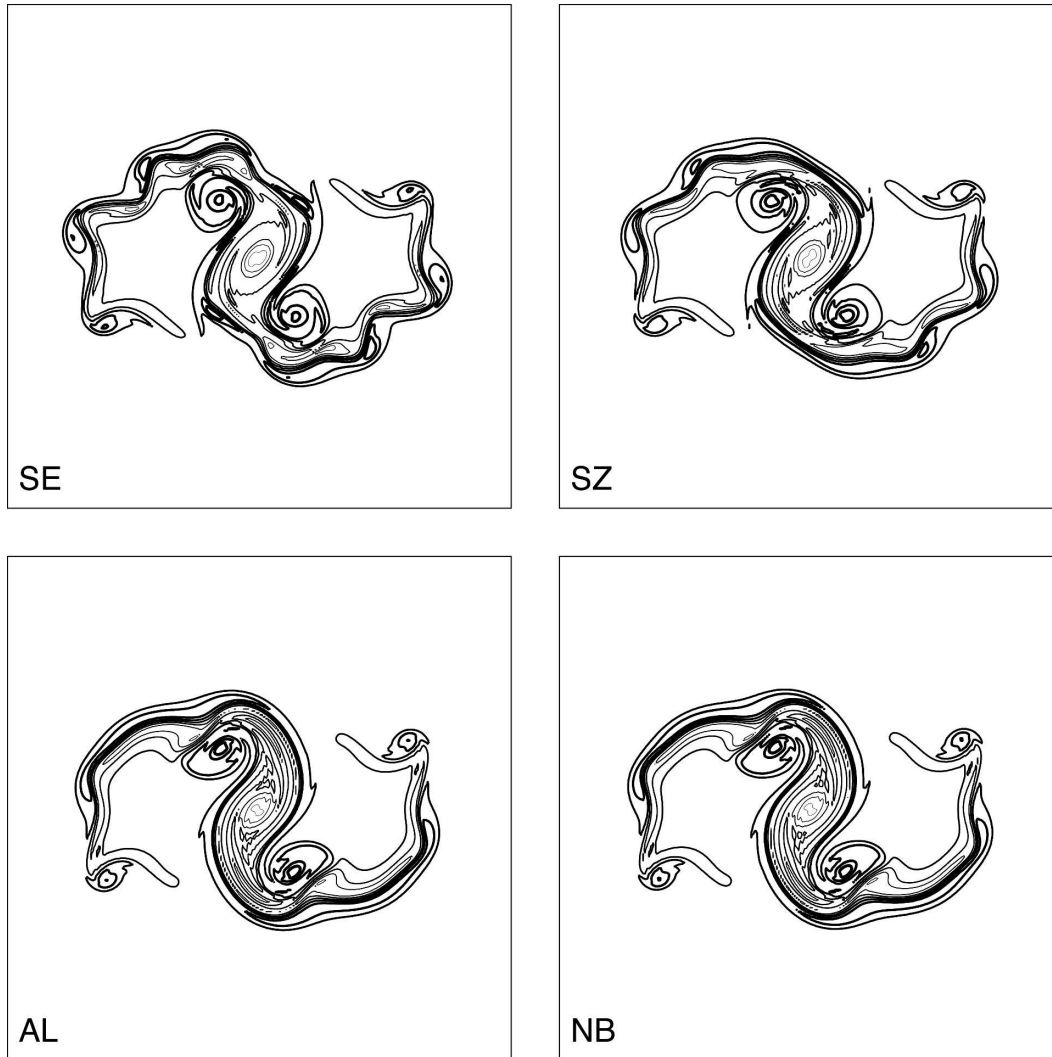


FIG. 6. The potential vorticity field in four numerical solutions of the viscous shallow-water equations that began from the same, geostrophically balanced initial conditions. All of the solutions correspond to a spatial resolution of 256×256 grid points. However, the two solutions (AL and NB) that conserve both energy and potential enstrophy more closely resemble the solutions of Fig. 7, which have twice the resolution.

there is an easy way to extend (3.15) to fourth-order accuracy. Let (3.15a) be rewritten as

$$\frac{d\zeta_0}{dt} = \left[\frac{d\zeta_0}{dt} \right]_{\Delta}, \quad (5.1)$$

where the right-hand side stands for the sum of (3.9) and (3.11). Then (5.1) implies

$$\frac{d\zeta_{ij}}{dt} = [J(q, \chi) - \nabla \cdot (q \nabla \gamma)]_{ij} + A \Delta^2, \quad (5.2)$$

where the square bracket represents the exact value at grid point ij , and the last term represents the truncation error in (3.9) and (3.11). The coefficient A is a complicated expression involving the derivatives of q , χ , γ , all

evaluated at ij . Now consider the finite-difference approximation

$$\frac{d\zeta_0}{dt} = \left[\frac{d\zeta_0}{dt} \right]_{2\Delta} \quad (5.3)$$

in which the right-hand side stands for the sum of (3.9) and (3.11) with Δ replaced by 2Δ and with the variables evaluated at twice the distance, but in the same direction, as before. For example, in (5.3) χ_2 means $\chi_{i+2, j+2}$ instead of $\chi_{i+1, j+1}$. Thus the Eq. (5.3) corresponds to the application of (5.1) on a square grid with half the original resolution. Clearly (5.3) implies (5.2) with Δ replaced by 2Δ , and no change in A . It follows that the finite-difference formula

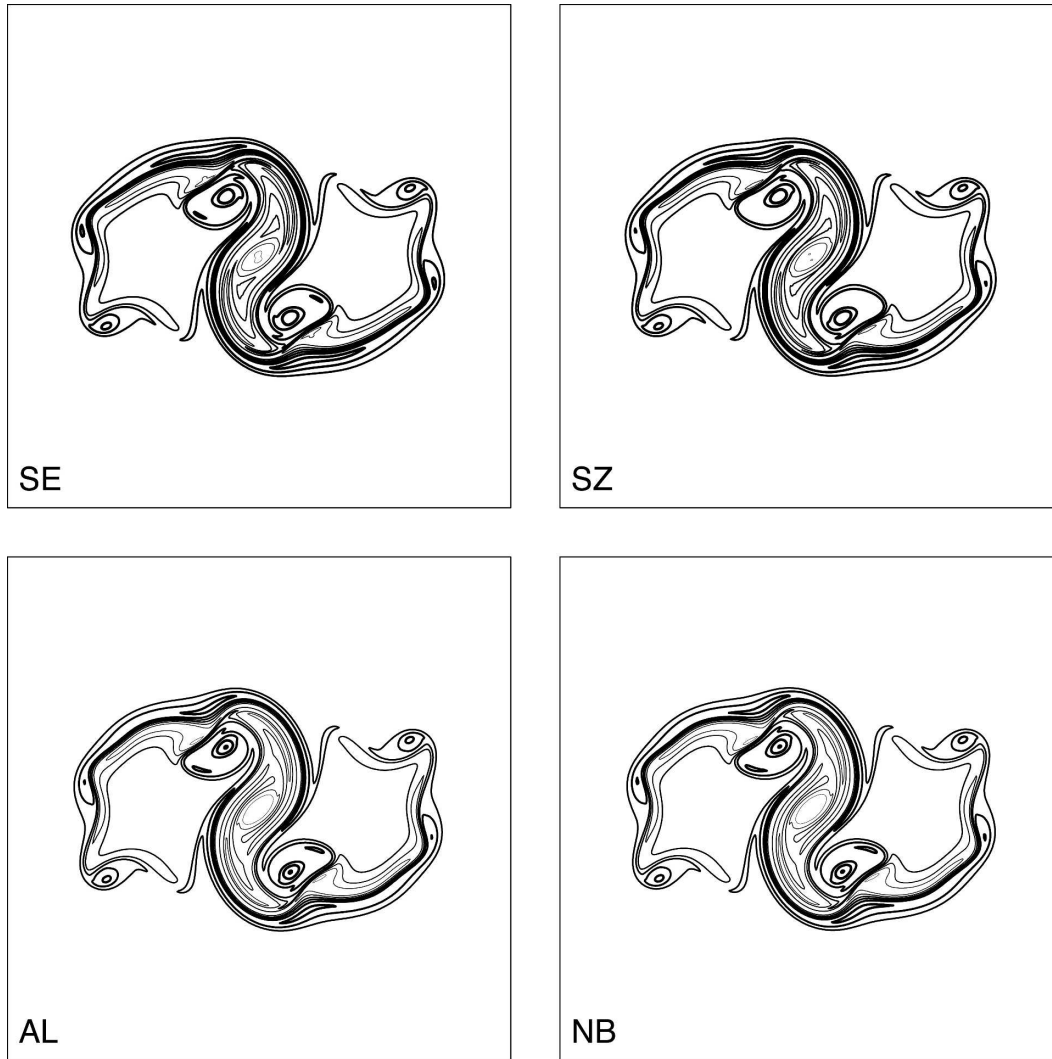


FIG. 7. The same as Fig. 6, but with a higher resolution of 512×512 grid points.

$$\frac{d\zeta_0}{dt} = \frac{4}{3} \left[\frac{d\zeta_0}{dt} \right]_{\Delta} - \frac{1}{3} \left[\frac{d\zeta_0}{dt} \right]_{2\Delta} \quad (5.4)$$

has fourth-order accuracy in Δ . Similar steps apply to (3.15b) and (3.15c). These more accurate approximations to (2.8) conserve exactly the same quantities as the second-order equations given explicitly in section 2, but the complete scheme remains only second-order accurate until we replace the energy (3.17) by a fourth-order approximation to (3.16). Fourth-order analogs of (3.19) and (3.20) would follow from that. However, improvements in the accuracy of the brackets are quite independent from improvements in the accuracy of the Hamiltonian, and in fact each of (2.13)–(2.15) can be treated independently. That is, each of the Jacobian terms in (2.8) may be handled differently from all the

remaining terms; it only matters that each of (2.13)–(2.15) retain its property of complete antisymmetry. The trick (5.4) depends critically on the fact that the potential enstrophy (3.1) does not itself involve finite differences, and therefore could not be applied to the scheme derived by Arakawa and Lamb (1981). This seems to be another advantage of the formulation in terms of ζ , μ , and h .

Next we apply the methods of sections 2 and 3 to a mesh composed of arbitrarily drawn triangles. The results extend to an arbitrary polygonal mesh. In the case of nonequilateral triangles, we must carefully distinguish between the functional derivatives and ordinary derivatives with respect to the values at mesh points. This distinction was unnecessary on the regular grid of section 3. For example, the triangular-mesh analog of (3.1) is

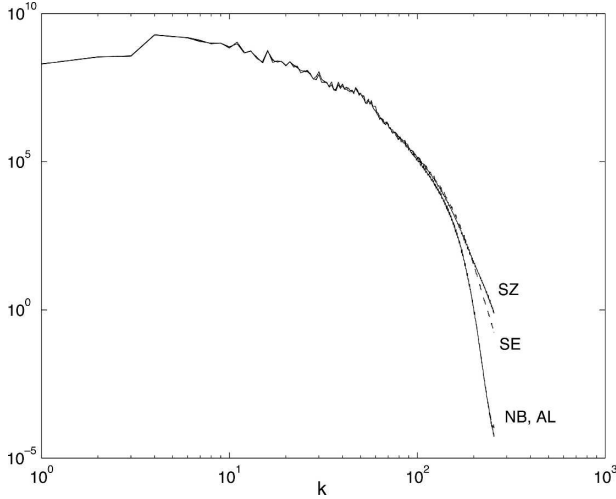


FIG. 8. The enstrophy spectra of the solutions depicted in Fig. 7. The spectra of the doubly conservative schemes AL and NB show the least enstrophy at high wavenumbers, and are nearly identical.

$$Z = \frac{1}{2} \sum_{\text{triangles}} \Omega_{123} \frac{1}{3} (h_1 q_1^2 + h_2 q_2^2 + h_3 q_3^2), \quad (5.5)$$

where the sum is over all the triangles in the mesh, and Ω_{123} is the area of the triangle with vertices labeled 1, 2, 3. Refer to Fig. 9. We define the functional derivative

$$\frac{\delta Z}{\delta \zeta_i} \equiv \frac{1}{\Omega_i} \frac{\partial Z}{\partial \zeta_i} = q_i \quad (5.6)$$

where the subscript denotes a particular mesh point, and Ω_i is the area associated with this meshpoint, namely, one-third the area of all the adjoining triangles. Similarly, of course, $\delta Z / \delta h_i = -1/2 q_i^2$ and $\delta Z / \delta \mu_i = 0$. The distinction between $\delta Z / \delta \zeta_i$ and $\partial Z / \partial \zeta_i$ was unimportant in section 3, because all the grid points had the same associated area, namely Δ^2 .

To obtain the triangular-mesh analogs of (3.15), we must replace the Nambu brackets (2.13)–(2.15) by finite-difference approximations on each triangle, being careful to maintain the critical antisymmetry properties. If $A(x, y)$, $B(x, y)$, and $C(x, y)$ depend linearly on x and y , it follows that

$$\begin{aligned} \iint_{\text{triangle}} dx AJ(B, C) &= \frac{1}{6} (A_1 + A_2 + A_3)(B_1 C_2 + B_2 C_3 \\ &+ B_3 C_1 - B_1 C_3 - B_3 C_2 - B_2 C_1) \end{aligned} \quad (5.7)$$

where the subscripts denote the vertex values in Fig. 9. Therefore [cf. (3.6)]

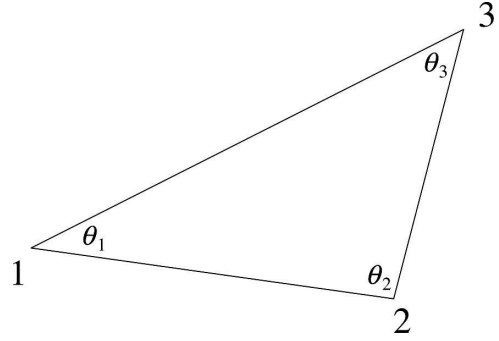


FIG. 9. A single triangle with corners numbered as in the text.

$$\begin{aligned} \{F, H, Z\}_{\zeta\zeta\zeta} &\rightarrow \sum_{\text{triangles}} \frac{1}{18} \left(\frac{\delta Z}{\delta \zeta_1} + \frac{\delta Z}{\delta \zeta_2} + \frac{\delta Z}{\delta \zeta_3} \right) \\ &\left(\frac{\delta F}{\delta \zeta_1} \frac{\delta H}{\delta \zeta_2} + \frac{\delta F}{\delta \zeta_2} \frac{\delta H}{\delta \zeta_3} + \frac{\delta F}{\delta \zeta_3} \frac{\delta H}{\delta \zeta_1} - \frac{\delta F}{\delta \zeta_1} \frac{\delta H}{\delta \zeta_3} \right. \\ &\left. - \frac{\delta F}{\delta \zeta_3} \frac{\delta H}{\delta \zeta_2} - \frac{\delta F}{\delta \zeta_2} \frac{\delta H}{\delta \zeta_1} \right) + \text{cyc}(F, H, Z) \end{aligned} \quad (5.8)$$

is a logical, antisymmetric, finite-difference approximation to (2.14) and (3.6) on the triangular mesh. Equation (5.8) is very closely related to the method used by Salmon and Talley (1989) to generalize Arakawa’s Jacobian to a triangular mesh. Since Z does not depend on μ , we may approximate (2.13) more simply, as

$$\begin{aligned} \{F, H, Z\}_{\mu\mu\zeta} &\rightarrow \sum_{\text{triangles}} \frac{1}{6} (q_1 + q_2 + q_3) \\ &\left(\frac{\delta F}{\delta \mu_1} \frac{\delta H}{\delta \mu_2} + \frac{\delta F}{\delta \mu_2} \frac{\delta H}{\delta \mu_3} + \frac{\delta F}{\delta \mu_3} \frac{\delta H}{\delta \mu_1} \right. \\ &\left. - \frac{\delta F}{\delta \mu_1} \frac{\delta H}{\delta \mu_3} - \frac{\delta F}{\delta \mu_3} \frac{\delta H}{\delta \mu_2} - \frac{\delta F}{\delta \mu_2} \frac{\delta H}{\delta \mu_1} \right). \end{aligned} \quad (5.9)$$

The bracket (5.8) is analogous to (3.8); (5.9) is analogous to (3.2). The bracket (5.8) conserves H and Z by antisymmetry; (5.9) conserves H by antisymmetry, and Z because $\delta Z / \delta \mu_i = 0$. It only remains to discretize (2.15).

The estimate (3.10) of (2.15) corresponds to a single differencing operator applied along every edge of every square grid box. We suppose that each triangle contributes a weighted sum of this same operator applied to each of its three edges. We choose the three weights to make our estimate of (2.15) agree with (2.4), after contraction with Z , in the limit of small triangles. Omitting details, we obtain the approximation

$$\{F, H, Z\}_{\zeta\mu h} \rightarrow \sum_{\text{triangles}} -\frac{1}{2} \cot\theta_3 \frac{1}{(q_2 - q_1)} \left[\left(\frac{\delta F}{\delta \mu_2} - \frac{\delta F}{\delta \mu_1} \right) \left(\frac{\delta H}{\delta \zeta_2} - \frac{\delta H}{\delta \zeta_1} \right) - \left(\frac{\delta H}{\delta \mu_2} - \frac{\delta H}{\delta \mu_1} \right) \left(\frac{\delta F}{\delta \zeta_2} - \frac{\delta F}{\delta \zeta_1} \right) \right] \left(\frac{\delta Z}{\delta h_2} - \frac{\delta Z}{\delta h_1} \right) + \text{cyc}(1, 2, 3) + \text{cyc}(F, H, Z), \tag{5.10}$$

where once again the integers refer to the vertices of the triangle in Fig. 9. The permutations $\text{cyc}(1, 2, 3)$ correspond to summation over the sides of each triangle. Thus, the full set of permutations in (5.10) corresponds to nine terms of the form explicitly given in (5.10). It is straightforward to check that (5.10) converges to (2.15) in the limit of small triangles.

Now let 0 denote an arbitrary node on the triangular mesh, as shown in Fig. 10. Then setting $F = \zeta_0, \mu_0, h_0$ in $dF/dt = \{F, H, Z\}$, where $\{F, H, Z\}$ is the sum of (5.8), (5.9), and (5.10), we obtain the analogs of (3.15) on the triangular mesh:

$$\begin{aligned} \frac{d\zeta_0}{dt} &= \frac{1}{6\Omega_0} \sum_n q_n (\chi_{n+1} - \chi_{n-1}) \\ &+ \frac{1}{4\Omega_0} \sum_n (\cot a_{n-1} + \cot b_{n+1}) (q_0 + q_n) (\gamma_0 - \gamma_n) \end{aligned} \tag{5.11a}$$

$$\begin{aligned} \frac{d\mu_0}{dt} &= \frac{1}{6\Omega_0} \sum_n q_n (\gamma_{n+1} - \gamma_{n-1}) \\ &- \frac{1}{4\Omega_0} \sum_n (\cot a_{n-1} + \cot b_{n+1}) (q_0 + q_n) (\chi_0 - \chi_n) \\ &+ \frac{1}{2\Omega_0} \sum_n (\cot a_{n-1} + \cot b_{n+1}) (\Phi_0 - \Phi_n) \end{aligned} \tag{5.11b}$$

$$\frac{dh_0}{dt} = \frac{1}{2\Omega_0} \sum_n (\cot a_{n-1} + \cot b_{n+1}) (\gamma_0 - \gamma_n). \tag{5.11c}$$

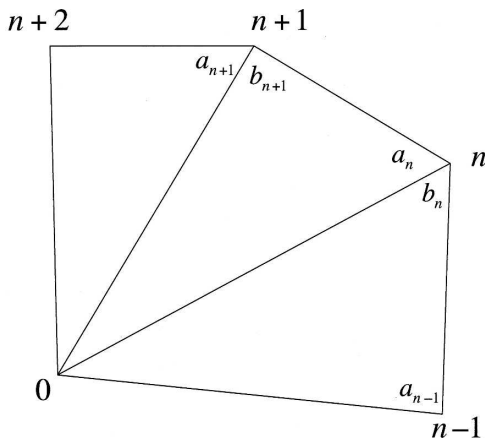


FIG. 10. An arbitrary nodal point, labeled 0, and some of its neighbors on an unstructured triangular mesh. The full set of neighbors forms an irregular polygon.

In (5.11), the sum over n corresponds to the sum over the triangles surrounding point 0, and $\chi_i \equiv -\delta H/\delta \zeta_i$, etc., as in section 3. The precise expression for χ_i, γ_i, h_i in terms of the ζ_i, μ_i, h_i depends on the precise choice of H , which determines the triangular-mesh analogs of (3.19) and (3.20). However, the dynamics (5.11) conserves the energy H and potential enstrophy (5.5) for any choice of H .

A regular hexagonal mesh corresponds to equilateral triangles with side s , all $a_i = b_i = \pi/3$, and $\Omega_0 = \sqrt{3}s^2/2$. Refer to Fig. 11. In the case of a regular hexagonal mesh (5.11) reduce to

$$\begin{aligned} \frac{d\zeta_0}{dt} &= \frac{1}{3\sqrt{3}s^2} [q_1(\chi_2 - \chi_6) + q_2(\chi_3 - \chi_1) + q_3(\chi_4 - \chi_2) \\ &+ q_4(\chi_5 - \chi_3) + q_5(\chi_6 - \chi_4) + q_6(\chi_1 - \chi_5)] \\ &+ \frac{1}{3s^2} [(q_0 + q_1)(\gamma_0 - \gamma_1) + (q_0 + q_2)(\gamma_0 - \gamma_2) \\ &+ (q_0 + q_3)(\gamma_0 - \gamma_3) + (q_0 + q_4)(\gamma_0 - \gamma_4) \\ &+ (q_0 + q_5)(\gamma_0 - \gamma_5) + (q_0 + q_6)(\gamma_0 - \gamma_6)] \end{aligned} \tag{5.12a}$$

$$\begin{aligned} \frac{d\mu_0}{dt} &= \frac{1}{3\sqrt{3}s^2} [q_1(\gamma_2 - \gamma_6) + q_2(\gamma_3 - \gamma_1) + q_3(\gamma_4 - \gamma_2) \\ &+ q_4(\gamma_5 - \gamma_3) + q_5(\gamma_6 - \gamma_4) + q_6(\gamma_1 - \gamma_5)] \\ &- \frac{1}{3s^2} [(q_0 + q_1)(\chi_0 - \chi_1) + (q_0 + q_2)(\chi_0 - \chi_2) \\ &+ (q_0 + q_3)(\chi_0 - \chi_3) + (q_0 + q_4)(\chi_0 - \chi_4) \\ &+ (q_0 + q_5)(\chi_0 - \chi_5) + (q_0 + q_6)(\chi_0 - \chi_6)] \\ &+ \frac{2}{3s^2} (6\Phi_0 - \Phi_1 - \Phi_2 - \Phi_3 - \Phi_4 - \Phi_5 - \Phi_6) \end{aligned} \tag{5.12b}$$

$$\frac{dh_0}{dt} = \frac{2}{3s^2} (6\gamma_0 - \gamma_1 - \gamma_2 - \gamma_3 - \gamma_4 - \gamma_5 - \gamma_6). \tag{5.12c}$$

The icosahedral method for grid generation on a sphere results in a geodesic mesh comprising 12 pentagons and an arbitrarily large number of nearly regular hexagons. See, for example, Randall et al. (2002). If the hexagons

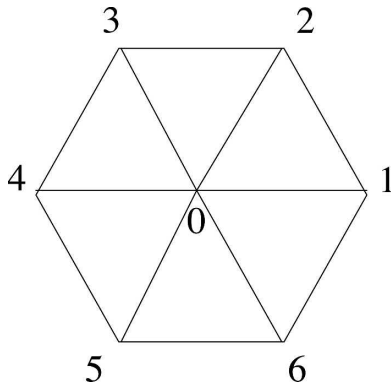


FIG. 11. An arbitrary nodal point and its six neighbors on a regular hexagonal grid.

are sufficiently regular, then one may use (5.12) instead of (5.11) with only a small geometrical distortion. The conserved potential enstrophy would be an approximation to (5.5) with Ω_{123} replaced by a global constant. However, the general Eq. (5.11) is needed for mesh points near the pentagons. Ringler and Randall (2002) have previously derived an energy- and potential-enstrophy-conserving shallow-water model based upon hexagons and pentagons. The model (5.12) is not equivalent to their model, and does not contain computational modes.

S05 showed how the algorithm of section 2 could be generalized to conserve energy and any single moment (4.4) of potential enstrophy. This result can be further generalized to arbitrary $G(q)$ in (1.13). However, numerical experiments not described here have shown that models designed to conserve Casimirs other than potential enstrophy generally behave very poorly in comparison with potential enstrophy-conserving models. Since, moreover, models designed to conserve $G(q) \neq q^2$ do not typically also conserve the circulation Z_1 , there seems little reason to consider anything besides potential-enstrophy-conserving models at this time.

6. Discussion

From the standpoint of differential equations, conservation laws arise from manipulations that typically include the product rule for derivatives. Unfortunately, the product rule does not generally carry over to discrete systems; try as we might, we will never get digital computers to respect it. However, in the strategy adopted in S05 and here, conservation laws are converted to antisymmetry properties that transfer easily to the discrete case; digital computers understand antisymmetry very well!

The general strategy of using antisymmetry properties to construct conservative numerical algorithms has been championed by McLachlan (2003). On the other hand, Nevir and Blender (1993) were apparently the first to realize that fluid mechanics could be posed as a Nambu bracket. The present work can be viewed as a confluence of these two ideas, or as a generalization of the method of Salmon and Talley (1989) to systems besides two-dimensional, incompressible flow. Although the present paper contributes only concrete examples to the general theory sketched in S05, it is hoped that it might inspire others, particularly those with computing skills and resources greater than the author, to adopt the antisymmetry approach to model development.

By the well-known analogy between the shallow-water equations and the hydrostatic primitive equations in isentropic coordinates (e.g., Salmon 1998, pp. 105–107), our results extend immediately to the three-dimensional, hydrostatic primitive equations. The evolution equations are essentially unchanged; the Hamiltonian acquires coupling terms between isentropic layers in the expression for potential energy. However, models of the earth's atmosphere and oceans should probably be based upon the nonhydrostatic primitive equations. In fact, Browning and Kreiss (1986), Salmon (1999), and Kuang et al. (2005) suggest that it is a good strategy to exaggerate nonhydrostatic effects by inserting a parameter much greater than unity in front of the acceleration term in the vertical momentum equation. This increases the horizontal scale of convection in both atmosphere and ocean, and the thickness of coastal boundary layers in the ocean, to the point where they can be more easily resolved by the model. S05 presents a Nambu bracket for the nonhydrostatic primitive equations, but that bracket is much more complicated than the shallow-water bracket. Finding its optimal discretization will likely require considerable effort.

Acknowledgments. This work was supported by National Science Foundation Grant OCE-0100868.

REFERENCES

- Abramopoulos, F., 1988: Generalized energy and potential enstrophy conserving finite difference schemes for the shallow water equations. *Mon. Wea. Rev.*, **116**, 650–662.
- Arakawa, A., 1966: Computational design for long-term numerical integration of the equations of fluid motion: Two-dimensional incompressible flow. Part I. *J. Comput. Phys.*, **1**, 119–143.
- , and V. R. Lamb, 1977: Computational design of the basic dynamical processes of the UCLA general circulation model. *Methods Comput. Phys.*, **17**, 173–265.

- , and —, 1981: A potential enstrophy and energy conserving scheme for the shallow water equations. *Mon. Wea. Rev.*, **109**, 18–36.
- Browning, G. L., and H.-O. Kreiss, 1986: Scaling and computation of smooth atmospheric motions. *Tellus*, **38A**, 295–313.
- Durran, D. R., 1991: The third-order Adams-Bashforth method: An attractive alternative to leapfrog time differencing. *Mon. Wea. Rev.*, **119**, 702–720.
- Kuang, Z., P. N. Blossey, and C. S. Bretherton, 2005: A new approach for three-dimensional cloud resolving simulations of large-scale atmospheric circulation. *Geophys. Res. Lett.*, **32**, L02809, doi:10.1029/2004GL021024.
- McLachlan, R. I., 2003: Spatial discretization of partial differential equations with integrals. *IMA J. Numer. Anal.*, **23**, 645–664.
- Morrison, P. J., 1998: Hamiltonian description of the ideal fluid. *Rev. Mod. Phys.*, **70**, 467–521.
- Nambu, Y., 1973: Generalized Hamiltonian dynamics. *Phys. Rev. D*, **7**, 2405–2412.
- Nevir, P., and R. Blender, 1993: A Nambu representation of incompressible hydrodynamics using helicity and enstrophy. *J. Phys.*, **26A**, L1189–L1193.
- Randall, D. A., 1994: Geostrophic adjustment and the finite-difference shallow-water equations. *Mon. Wea. Rev.*, **122**, 1371–1377.
- , T. D. Ringler, R. P. Heikes, P. Jones, and J. Baumgardner, 2002: Climate modeling with spherical geodesic grids. *Comp. Sci. Eng.*, **4**, 32–41.
- Ringler, T. D., and D. A. Randall, 2002: A potential enstrophy and energy conserving numerical scheme for the solution of the shallow-water equations on a geodesic grid. *Mon. Wea. Rev.*, **130**, 1397–1410.
- Sadourny, R., 1975: The dynamics of finite-difference models of the shallow-water equations. *J. Atmos. Sci.*, **32**, 680–689.
- Salmon, R., 1998: *Lectures on Geophysical Fluid Dynamics*. Oxford University Press, 372 pp.
- , 1999: Lattice Boltzmann solutions of the three-dimensional planetary geostrophic equations. *J. Mar. Res.*, **57**, 847–884.
- , 2004: Poisson-bracket approach to the construction of energy- and potential-enstrophy conserving algorithms for the shallow water equations. *J. Atmos. Sci.*, **61**, 2016–2036.
- , 2005: A general method for conserving quantities related to potential vorticity in numerical models. *Nonlinearity*, **18**, R1–16.
- , and L. D. Talley, 1989: Generalizations of Arakawa's Jacobian. *J. Comput. Phys.*, **83**, 247–259.
- Shepherd, T. G., 1990: Symmetries, conservation laws, and Hamiltonian structure in geophysical fluid dynamics. *Advances in Geophysics*, Vol. 32, Academic Press, 287–338.